Journal of Materials Chemistry C RSCPublishing

ARTICLE

Supporting Information for

Facile Fabrication of Color-Tunable and White Light Emitting Nano-Composite Films Based on Layered Rare-earth Hydroxides

Liangliang Liu,[a] Minghui Yu,[a] Jian Zhang,[b] Bingkai Wang,[a] Weisheng Liu,[a] and Yu Tang,*[a]

[a]Key Laboratory of Nonferrous Metal Chemistry and Resources Utilization of Gansu Province, State Key Laboratory of Applied Organic Chemistry, College of Chemistry and Chemical Engineering, Lanzhou University, Lanzhou 730000, P. R. China

[b]Department of Chemistry, University of Nebraska-Lincoln Lincoln, NE 68588-0304, USA

List of Contents

characteristic peaks of Tb^{3+} were observed by a cascaded energy transfer from host (LRH) to Tb via sensitizer SA. Spectra were obtained with excitation at 330 nm for NaSA, 365 nm for SA-LGdH and SA-LGdH:Tb.

Figure S11. Top-view SEM images of the nano-composite films containing different hybrid phosphors loadings (0.5 wt%, 1.0 wt%, 3 wt%, 10 wt%, respectively).

Figure S12. Tapping-mode AFM images of the nano-composite films containing different hybrid phosphors loadings (0.5 wt%, 1.0 wt%, 3 wt%, 10 wt%, respectively).

Table S3. Roughness of the nano-composite films containing different hybrid phosphors loadings (0.5 wt%, 1.0 wt%, 3.0 wt%, 5.0 wt%, 10 wt%).

Figure S13. Fluorescence microscope image of the nano-composite films containing different hybrid phosphors loadings (0.5 wt%, 1.0 wt%, 3.0 wt%, 10 wt%, respectively).

Figure S14. Schematic representation of the energy-transfer mechanism for SA-LGdH:$Tb_{0.5-x}Eu_x$ (x = 0 - 0.50).

Figure S15. Luminescence decays of $^5D_0$ of Eu^{3+} in samples PMMA@SA-LGdH:$Tb_{0.5-x}Eu_x$ (x = 0.0005, 0.001, 0.003, 0.005, 0.01; λ_{ex} = 365 nm, λ_{em} = 613 nm).

Figure S16. Luminescence decays of $^5D_4$ of Tb^{3+} in samples PMMA@SA-LGdH:$Tb_{0.5-x}Eu_x$ (x = 0, 0.0005, 0.001, 0.003, 0.005, 0.01; λ_{ex} = 365 nm, λ_{em} = 543 nm).

Figure S17. Excitation (black) and emission (red) spectra for Na_2BSB.

Figure S18. White light emission chromaticity chart principle diagram.

Figure S19. PL spectra (lift) and CIE diagram (right) of PMMA@SA/BSB-LGdH:$Tb_{0.497}Eu_{0.003}$ (SA/BSB = molar ratio of 200, 400, 600) nano-composite films which was excited by UV irradiation at different wavelengths.

Figure S20. PL intensities (I_{543}) of the PMMA@SA/BSB-LGdH:$Tb_{0.497}Eu_{0.003}$ nano-composite films which are excitated by λ_{ex} = 330, 340, 360 nm, respectively.

Table S4. CIE and the quantum yields of the PMMA@SA/BSB-LGdH:$Tb_{0.5-x}Eu_x$ (x = 0.001, 0.005, 0.008).

Characterization data

Table S1. Compositions of SA-LGdH:$Tb_{0.5-x}Eu_x$ (x = 0 - 0.5) from A to L incorporated with different mole rations of Tb/Eu and corresponding powder X-ray diffraction (PXRD) patterns data for the SA-LGdH:$Tb_{0.5-x}Eu_x$ (x = 0 - 0.5) samples.

	Mole ratio of multiple luminescent dopants				PXRD data	
Samples	Gd	Tb	Eu	SA	d_{002} (Å)	2θ (°)
a (x = 0)	0.4565	0.5435	–	0.552	14.52	5.654
b (x = 0.0005)	0.4570	0.5427	0.0003	0.567	15.18	5.938
c (x = 0.001)	0.4582	0.5411	0.0007	0.579	15.37	5.982
d (x = 0.003)	0.4715	0.563	0.0022	0.561	14.77	5.703
e (x = 0.005)	0.4720	0.5241	0.0039	0.575	15.13	5.889
f (x = 0.008)	0.4713	0.5229	0.0059	0.568	15.09	5.840
g (x = 0.01)	0.4709	0.5207	0.0084	0.573	14.94	5.738
h (x = 0.05)	0.4611	0.4970	0.0419	0.566	14.89	5.716
i (x = 0.15)	0.4843	0.3874	0.1283	0.569	15.03	5.819
j (x = 0.25)	0.4772	0.2833	0.2395	0.545	14.09	5.577
k (x = 0.35)	0.5063	0.1688	0.3248	0.581	15.10	5.879
l (x = 0.50)	0.5029	–	0.4971	0.584	14.97	5.747

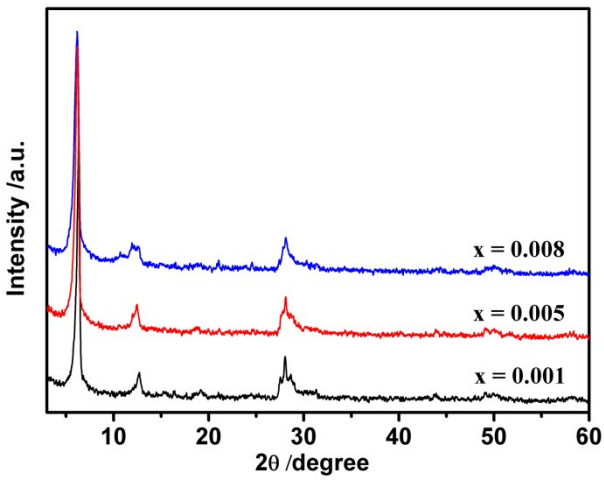

Figure S1. PXRD patterns of the SA/BSB-LGdH:$Tb_{0.5-x}Eu_x$ (molar ratio of SA/BSB = 500, x = 0.001, 0.005, 0.008).

Figure S1 shows PXRD patterns of SA/BSB-LGdH:$Tb_{0.5-x}Eu_x$ (SA/BSB = molar ratio of 500, x = 0.001, 0.005, 0.008) organic-inorganic hybrid phosphors. All the PXRD patterns of the cointercalation of SA and BSB into LRHs show the systematic shifts of the (*00l*) reflections toward lower diffraction angles. Such a systematic shifts and significant expansion demonstrate the intercalated structures. The absence of the peak at 2θ = 3.5° for BSB in the patterns of SA/BSB-LGdH:$Tb_{0.5-x}Eu_x$ (x = 0.001, 0.005, 0.008)may be attributed to the very low content of BSB in the hybrid phosphors.[S1] The results of the PXRD analysis demonstrate that the SA/BSB-LGdH:$Tb_{0.5-x}Eu_x$ (x = 0.001, 0.005, 0.008) hybrid phosphors show good crystallinity and are successfully synthesized.

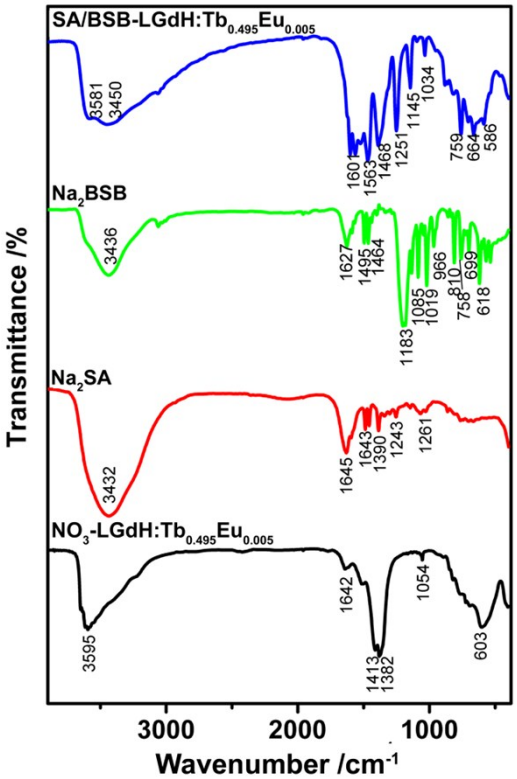

Figure S2. FT-IR measurements for NO_3-LGdH:$Tb_{0.495}Eu_{0.005}$, NaSA, Na_2BSB, SA/BSB-LGdH:$Tb_{0.495}Eu_{0.005}$.

The successful intercalation of the organic anion (SA and BSB) can be further confirmed by the FT-IR spectra as shown in Figure S2. The broad band at approximately 1378 cm^{-1} is characteristic of an uncoordinated nitrate anions in NO_3-LGdH:$Tb_{0.495}Eu_{0.005}$. In general, the strong, broad band at approximately 3595 cm^{-1} corresponds to O-H stretching vibrations (v_1 and v_3), whereas the band at 1642 cm^{-1} is assigned to the H-O-H bending mode (v_2); these results provide evidence for the presence of water molecules in the structure. After the organic anions (SA and BSB) were intercalated into the LGdH:$Tb_{0.495}Eu_{0.005}$ layer, the adsorption of the nitrate anions was completely disappeared and the emergence of absorption at 1596 cm^{-1} is assigned to the bending vibration of the C=O group. In addition, the symmetry and asymmetry absorption bands of S=O bond in sulfonate group were observed at 1145 and 1034 cm^{-1} respectively, demonstrated that the SA and BSB anions were intercalated into the LGdH:$Tb_{0.495}Eu_{0.005}$ layer.

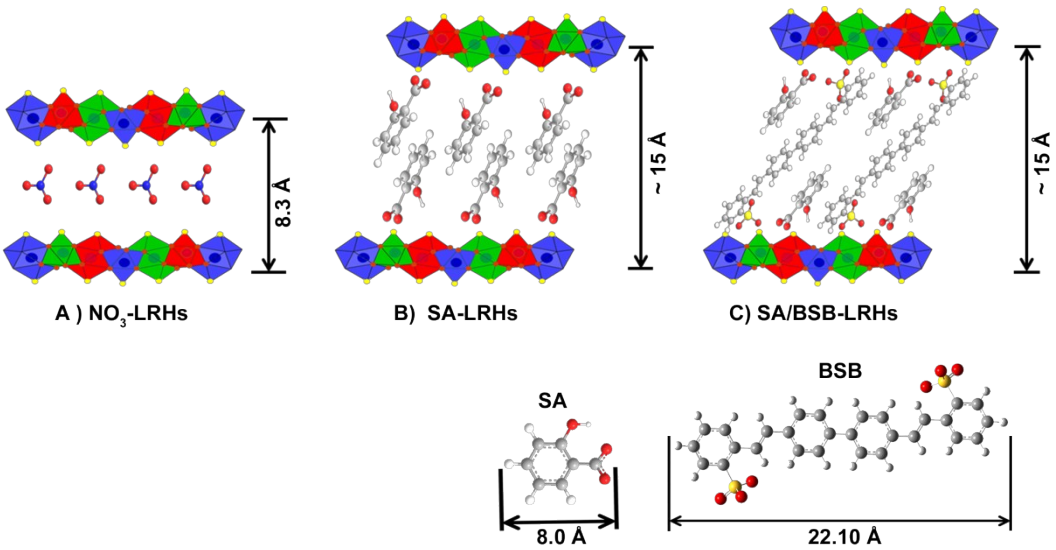

Figure S3. Schematic representation of the proposed arrangements of gallery species between the layers.

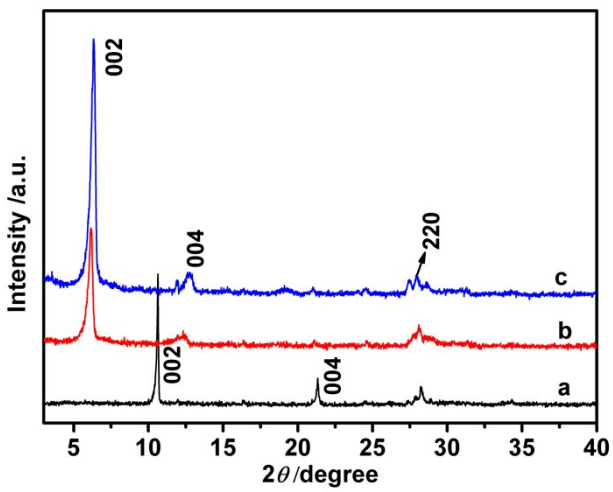

Figure S4. PXRD patterns of the as-obtained (a) NO_3^- product and those formed after anion exchange with (b) SA and (c) SA/BSB (molar ratio of SA/BSB = 500).

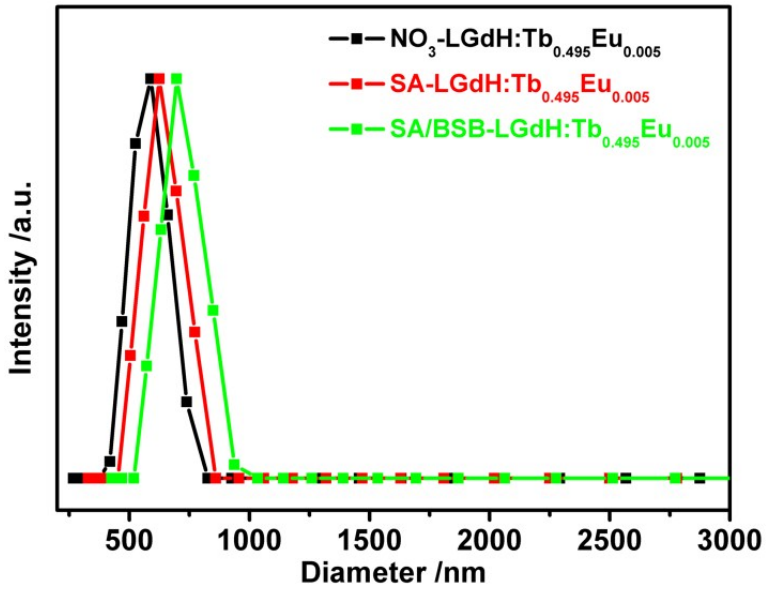

Figure S5. DLS plots of the NO_3-LGdH:$Tb_{0.495}Eu_{0.005}$, SA-LGdH:$Tb_{0.495}Eu_{0.005}$, SA/BSB-LGdH:$Tb_{0.495}Eu_{0.005}$.

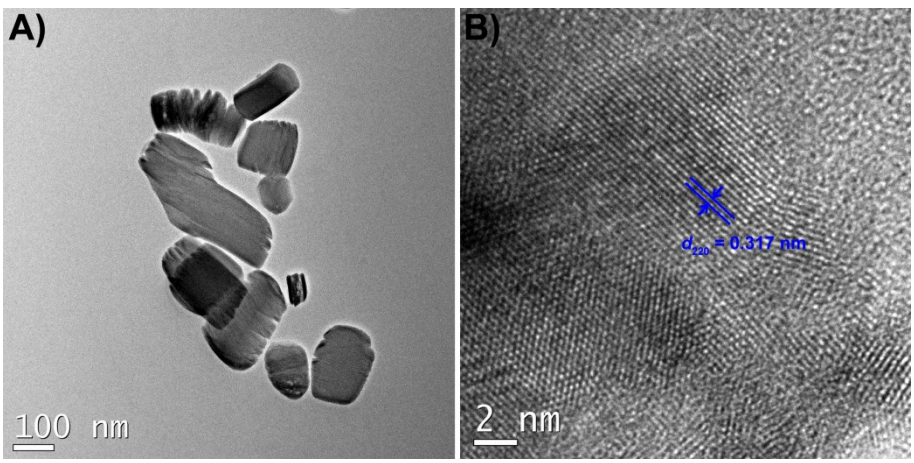

Figure S6. A) TEM image, B) HRTEM image and C) corresponding SAED pattern of SA/BSB-LGdH:$Tb_{0.495}Eu_{0.005}$.

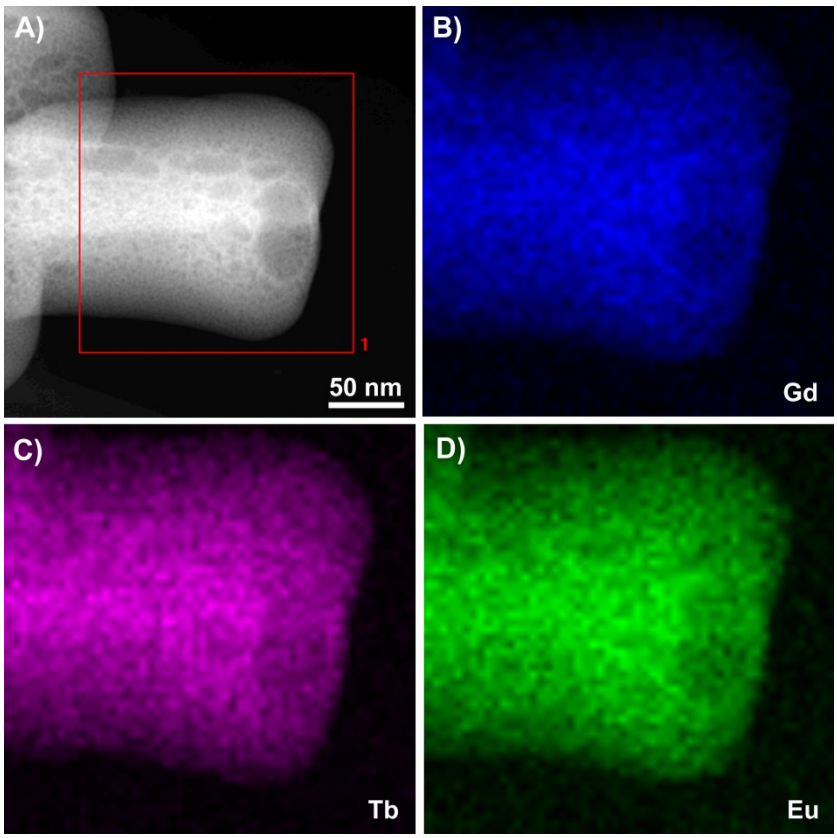

Figure S7. DF-STEM and corresponding elemental mapping images of the NO_3-LGdH:$Tb_{0.25}Eu_{0.25}$.

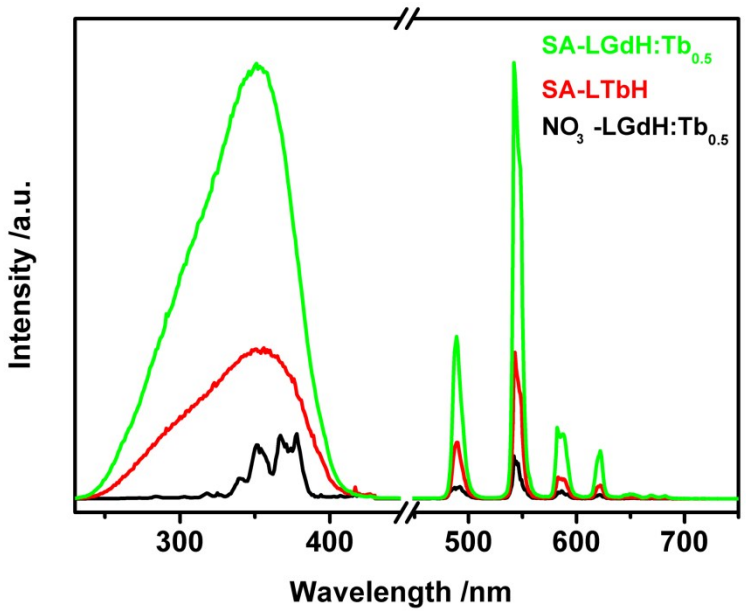

Figure S8. Excitation (left) and emission (right) spectra of NO_3-LGdH:$Tb_{0.5}$, SA-LTbH and SA-LGdH:$Tb_{0.5}$.

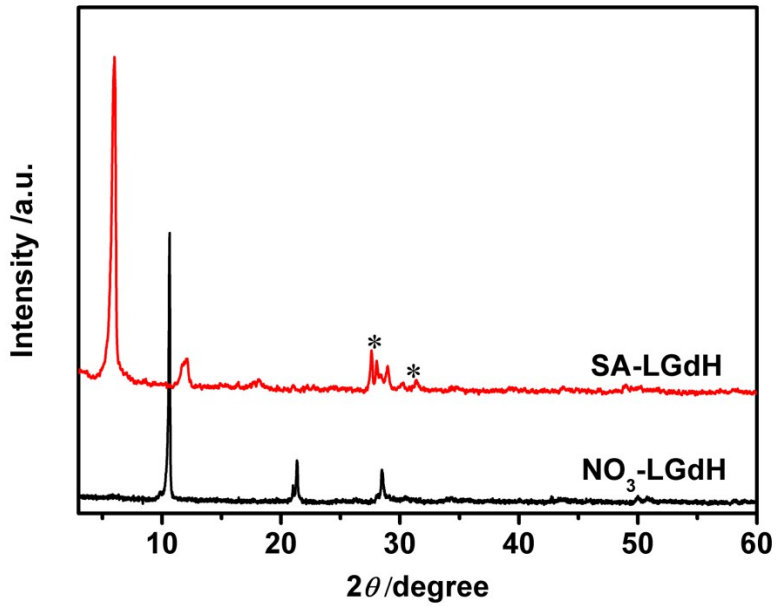

Figure S9. PXRD patterns of NO_3-LGdH and SA-LGdH (*: $NaNO_3$ impurity).

Table S2. Characterization data for the organic sensitizers exchange derivatives of NO_3-LGdH.

Comp.	Composition	Elemental analysis	
		Observed (%)	Calculated (%)
NO_3-LGdH	$Gd_2(OH)_5NO_3 \cdot H_2O$	Gd 64.8, N 2.3,H 1.5	Gd 65.6, N 2.9,H 1.5
SA-LGdH	$Gd_2(OH)_5SA \cdot H_2O$	C 15.83, H 1.96	C 15.67, H 1.88

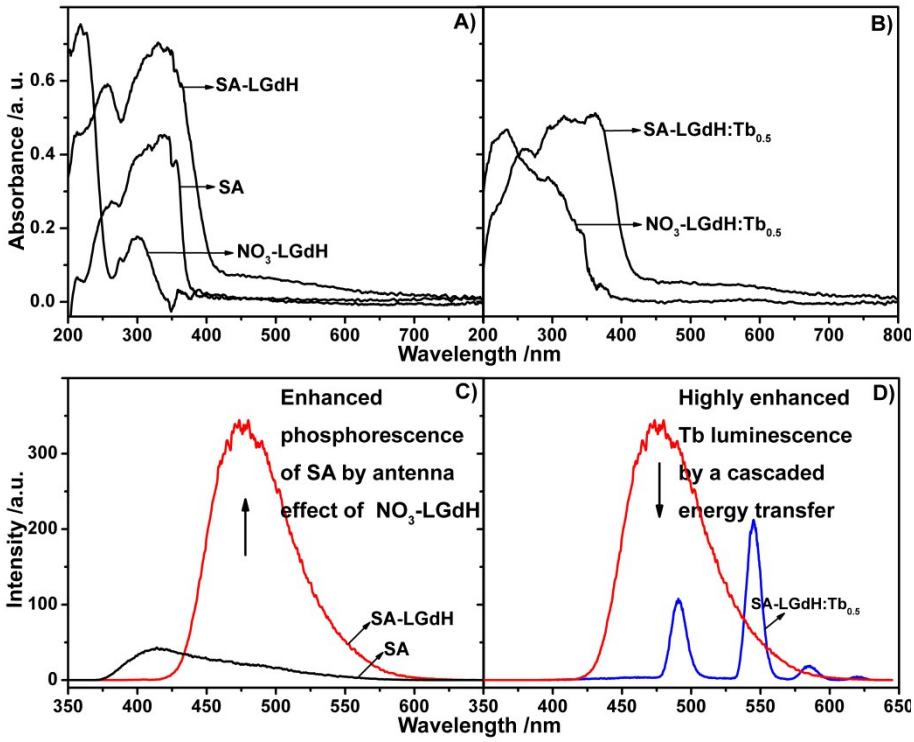

Figure S10. UV-vis absorption spectra of A) NaSA, NO_3-LGdH, SA-LGdH, B) NO_3-LGdH:$Tb_{0.5}$, SA-LGdH:$Tb_{0.5}$. Low temperature (77K) phosphorescence spectra of C) NaSA and SA-LGdH, phosphorescence of sensitizer SA was dramatically enhanced by NO_3-LGdH, c) When Tb^{3+} and Gd^{3+} ions exist simultaneously in the host, the phosphorescence emission from sensitizer SA was quenched, and characteristic peaks of Tb^{3+} were observed by a cascaded energy transfer from host (LRH) to Tb^{3+} via sensitizer SA. Spectra were obtained with excitation at 330 nm for NaSA, 365 nm for SA-LGdH and SA-LGdH:Tb.

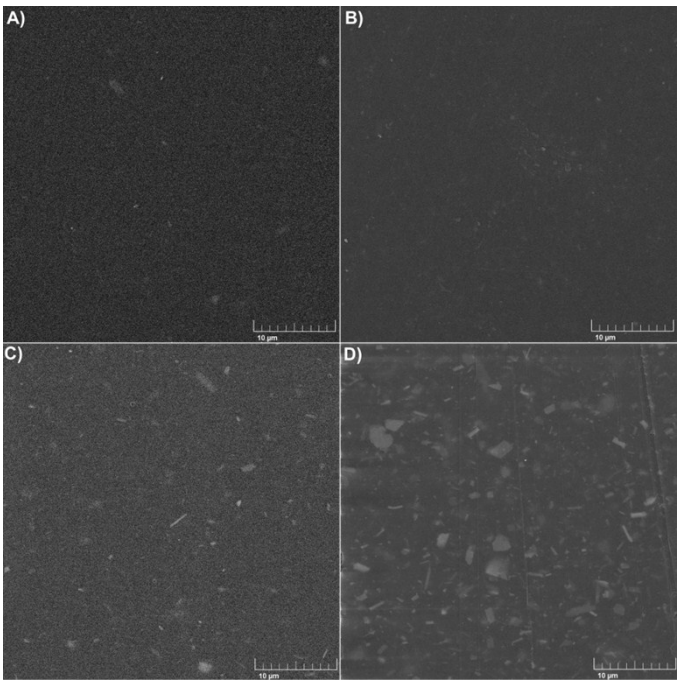

Figure S11. Top-view SEM images of the nano-composite films containing different hybrid phosphors loadings (0.5 wt%, 1.0 wt%, 3 wt%, 10 wt%, respectively).

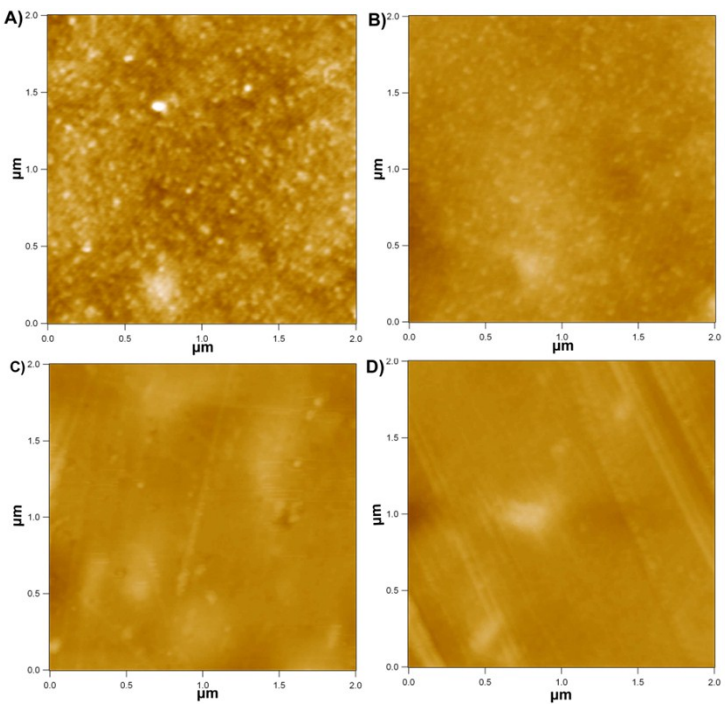

Figure S12. Tapping-mode AFM images of the nano-composite films containing different hybrid phosphors loadings (0.5 wt%, 1.0 wt%, 3 wt%, 10 wt%, respectively).

Table S3. Roughness of the nano-composite films containing different hybrid phosphors loadings (0.5 wt%, 1.0 wt%, 3.0 wt%, 5.0 wt%, 10 wt%).

Loadings (wt%)	0.5	1.0	3.0	5.0	10
RMS roughness (nm)	0.390	0.705	0.852	1.817	2.358

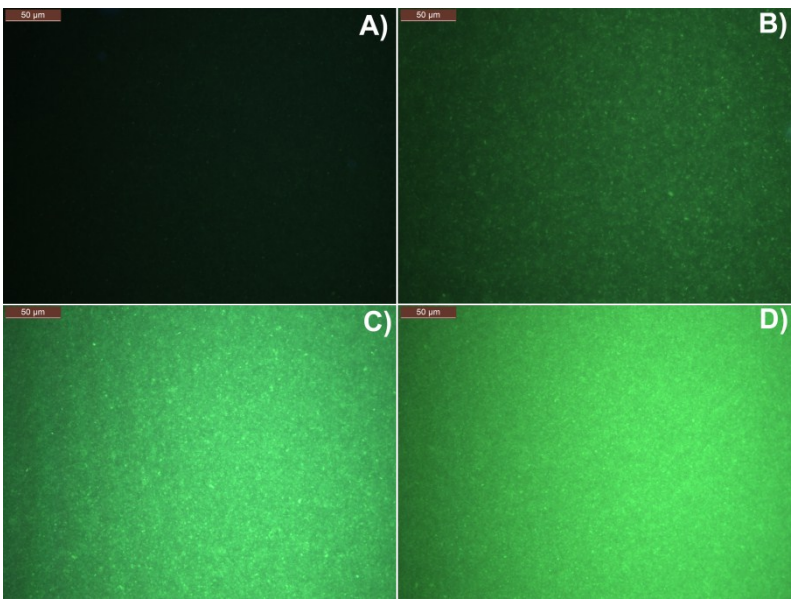

Figure S13. Fluorescence microscope images of the nano-composite films containing different hybrid phosphors loadings (0.5 wt%, 1.0 wt%, 3.0 wt%, 10 wt%, respectively).

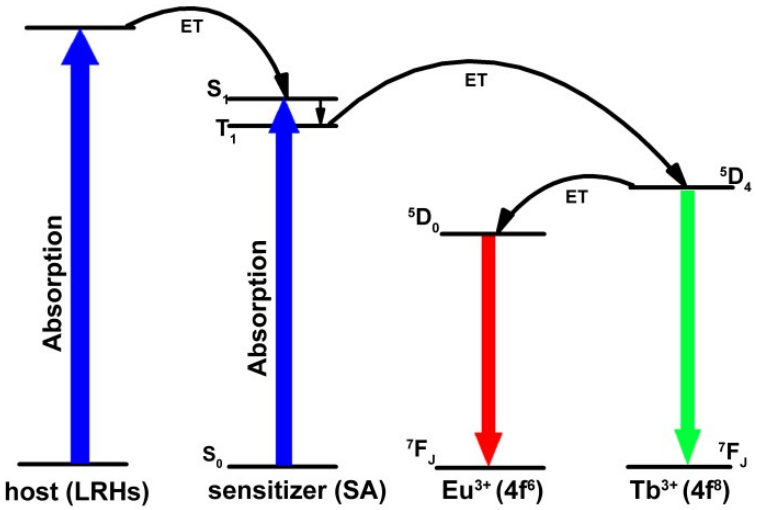

Figure S14. Schematic representation of the energy-transfer mechanism for SA-LGdH:$Tb_{0.5-x}Eu_x$ (x = 0 - 0.50).

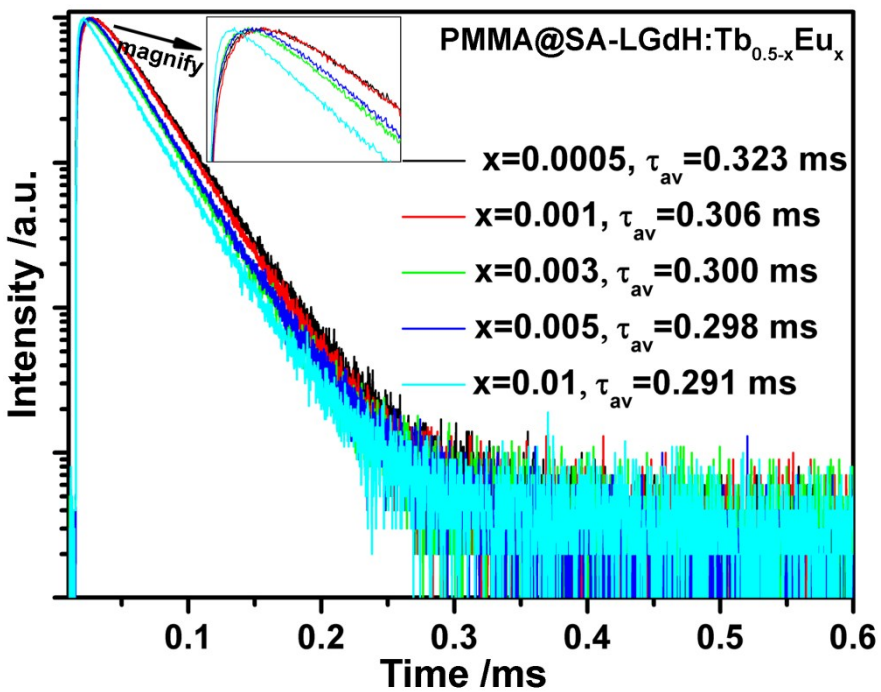

Figure S15. Luminescence decays of $^5D_0$ of Eu^{3+} in samples PMMA@SA-LGdH:$Tb_{0.5-x}Eu_x$ (x = 0.0005, 0.001, 0.003, 0.005, 0.01; λ_{ex} = 365 nm, λ_{em} = 613 nm).

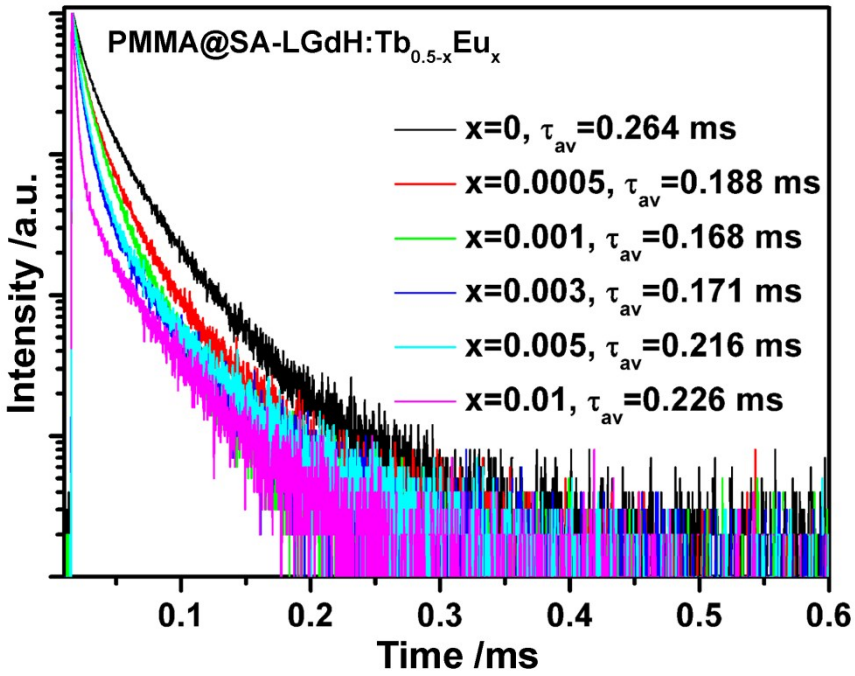

Figure S16. Luminescence decays of $^5D_4$ of Tb^{3+} in samples PMMA@SA-LGdH:$Tb_{0.5-x}Eu_x$ (x = 0, 0.0005, 0.001, 0.003, 0.005, 0.01; λ_{ex} = 365 nm, λ_{em} = 543 nm).

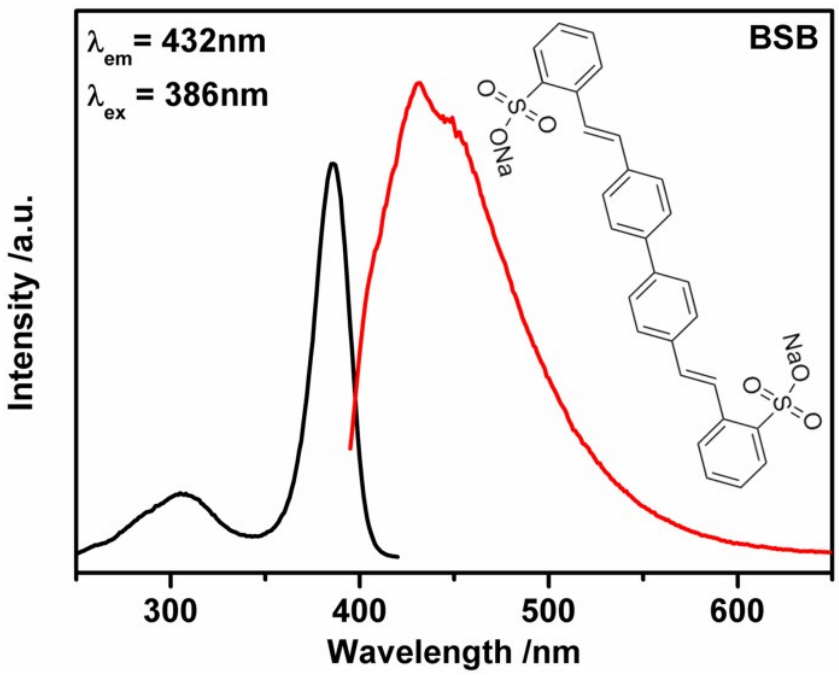

Figure S17. Excitation (black) and emission (red) spectra for BSB.

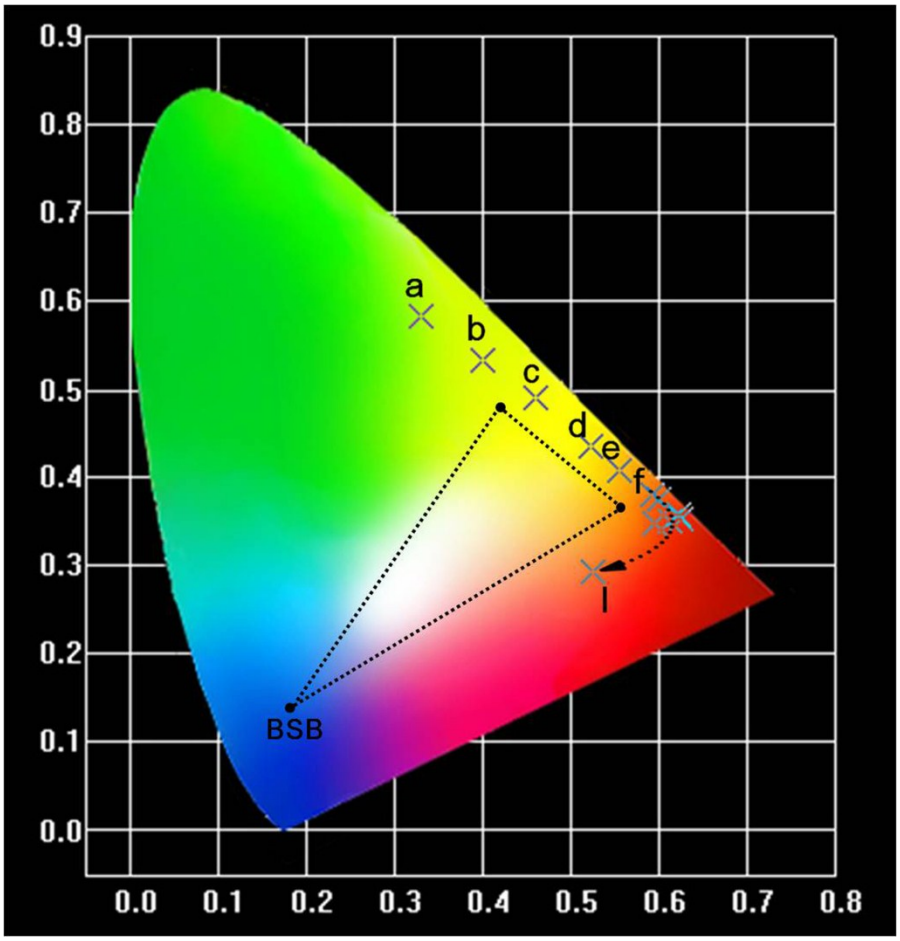

Figure S18. White light emission chromaticity chart principle diagram.

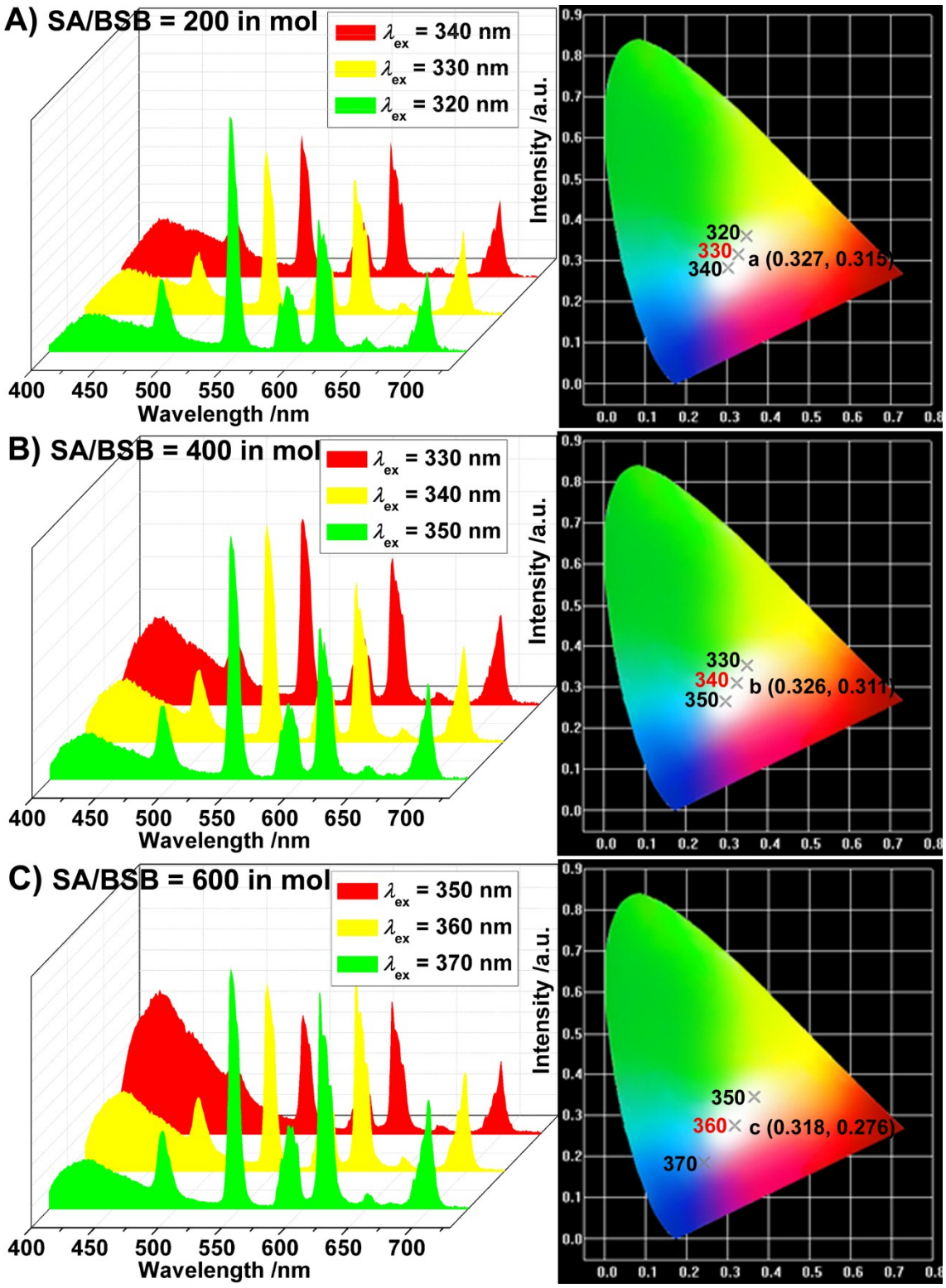

Figure S19. PL spectra (left) and CIE diagram (right) of the PMMA@SA/BSB-LGdH:$Tb_{0.497}Eu_{0.003}$ nano-composite films which was excited by UV irradiation at different wavelengths, molar ratio of SA/BSB = A) 200, B) 400, C) 600, respectively

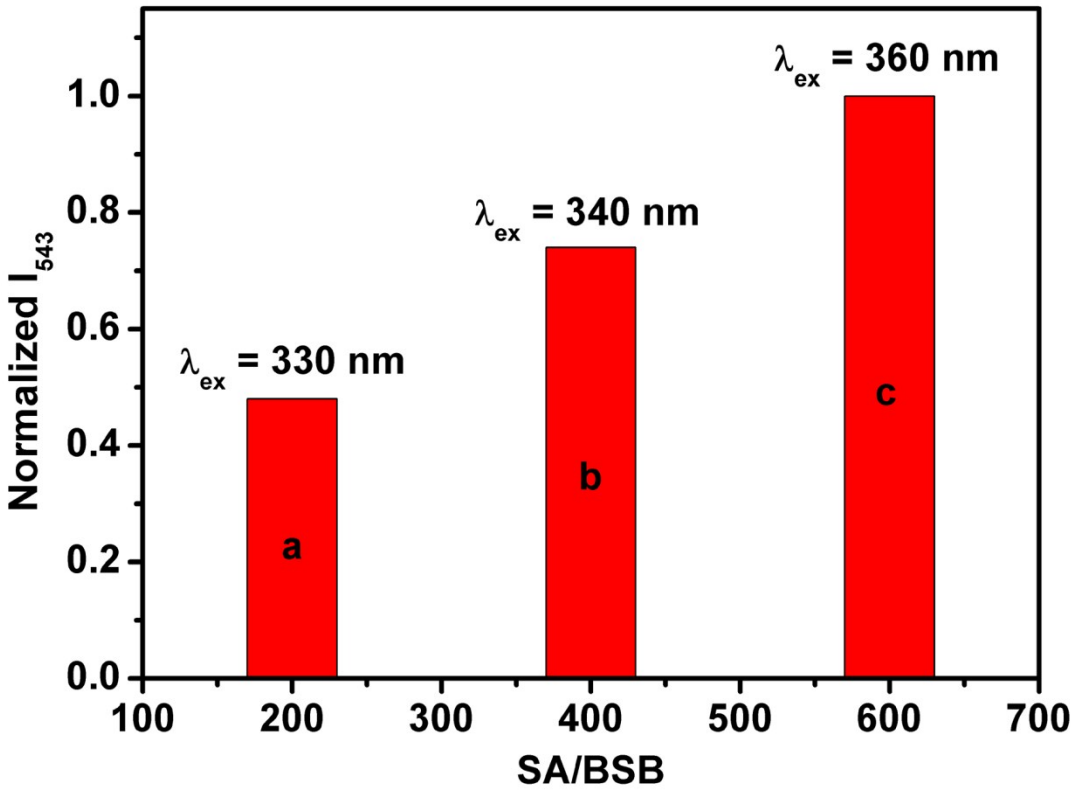

Figure S20. PL intensities (I_{543}) of the PMMA@SA/BSB-LGdH:$Tb_{0.497}Eu_{0.003}$ nano-composite films which are excitated by λ_{ex} = 330, 340, 360 nm, respectively.

Table S4. CIE and the quantum yields of the PMMA@SA/BSB-LGdH:$Tb_{0.5-x}Eu_x$ (x = 0.001, 0.005, 0.008).

Samples	0.001	0.005	0.008
λ_{ex} /nm	CIE (x, y)	CIE (x, y)	CIE (x, y)
350	(0.317, 0.341)	(0.385, 0.343)	(0.450, 0.329)
355	(0.291, 0.315)	(0.354, 0.323)	(0.423, 0.315)
360	(0.267, 0.283)	(0.328, 0.298)	(0.389, 0.298)
365	(0.233, 0.249)	(0.284, 0.266)	(0.343, 0.275)
370	(0.214, 0.237)	(0.242, 0.235)	(0.293, 0.252)
Φ(%)	12.3[a]	11.4[b]	11.6[c]

[a] λ_{ex} = 355 nm, [b] λ_{ex} = 355 nm, [c] λ_{ex} = 365 nm.

Reference

[S1] T. Wen, X. L. Wu, X. L. Tan, X. K. Wang, A. W. Xu, *ACS Appl. Mater.& Interfaces,* 2013*, 5,* 3304-3311.

[S2] K.-H. Lee, S.-H. Byeon, *Eur. J. Inorg. Chem.,* 2009, 4727-4732.

